Extreme Mechanics Letters 64 (2023) 102090

Contents lists available at ScienceDirect

Extreme Mechanics Letters

journal homepage: www.elsevier.com/locate/eml

V-shaped double peeling of films from curved rigid substrates

Ce Sun [a], Jian Sun [a], Fei Jia [b], Yanju Liu [b], Jinsong Leng [a,*]

[a] Center for Composite Materials and Structures, Science Park of Harbin Institute of Technology (HIT), P.O. Box 3011, No. 2 YiKuang Street, Harbin 150080, People's Republic of China

[b] Department of Astronautical Science and Mechanics, Harbin Institute of Technology (HIT), P.O. Box 301, No. 92 West Dazhi Street, Harbin 150001, People's Republic of China

ARTICLE INFO

Keywords:
Hyperelastic film
V-shaped double peeling
Adhesion of curved substrate
Adhesive energy release rate

ABSTRACT

The peeling phenomenon of films from rigid substrates has been extensively studied, most of which have focused on flat substrates. However, in natural environments, curved substrates with irregular geometries are more prevalent. In this study, the peeling behavior of films from curved rigid substrates is studied. The theoretical model for V-shaped double peeling (VDP) of hyperelastic films from semi-cylindrical substrates has been proposed based on the Griffith's energy equilibrium theory. An implicit mathematical expression of the relationship between vertical displacement and peeling length is obtained. The peeling length, peeling angle, peeling force and energy change during the peeling process are analyzed and discussed. Subsequently, experimental tests of V-shaped double peeling are carried out affirming the reliability and accuracy of the model. Finally, a simple and efficient new method for evaluating the adhesive energy release rate is proposed.

1. Introduction

The adhesion of soft materials is common in industrial and natural environments and it is significant to study the adhesion and debonding mechanisms of soft materials for advancing the fields of biomedical engineering, soft robots and flexible electronics [1–5]. Some extraordinary creatures, such as geckos, beetles and other adhesion masters, can rapidly crawl across vertical rocks and ceilings surfaces, which has inspired numerous studies on bio-inspired adhesive systems [6–9]. The adhesion mechanisms of these organisms rely on multi-layered V-shaped structures [10–19].

On a macroscopic scale, as shown in Fig. 1(a), to avoid detachment, geckos form the V-shaped structure relative to their legs or toes [10,11,20,22,23]. On a microscopic scale, as shown in Fig. 1(b), their enhanced adhesion ability and rapid switches between attachment and detachment are primarily attributed to multi-layered structures consisting of contralateral legs, toes and even setae [12,13]. As a basic unit of multi-layered structures, V-shaped structure is used for understanding adhesion mechanisms of organisms.

Most existing studies have been focused on VDP from flat substrates, as shown in Fig. 1(c). In 2011, Pugno [12] proposed a multiple peeling theory model for linear elastic films peeling from flat substrates based on the Kendall [24] single peeling theory. This research revealed the existence of a limiting peeling angle, which corresponds to the critical peeling force. And both limiting peeling angle and critical peeling force are related to the modulus of the film, geometry and interfacial energy. The situation in which peeling force exceeds critical value is not further discussed in this study. This theory was subsequently applied to the analysis of VDP of elastic tapes and axisymmetric peeling of films in 2013, and the situation in which peeling force exceeds critical value were studied [11]. Specifically, the peeling angle stabilized at a limit value with the advancement of the peeling process, which also depended on the geometry, elastic modulus and interface energy. In other words, VDP from flat substrates presents a self-similar situation. L. Afferrante et al. [14] further investigated peeling stability and demonstrated that the presence of pre-tension does not change the stability behavior of the system but significantly affects the peeling force. Two experimental studies on the mechanism of VDP [10,15] provided additional validation for the effectiveness of the VDP theory model in 2017 and 2018. Gialamas et al. [25] introduced the cohesion model into the VDP system by setting the cohesion region, which is significant to the theoretical study of VDP, because this cohesion model may be suitable as an approximation of more complex interaction for soft film peeling. It is also found that for VDP, after the initial stage of unstable peeling, peeling behavior gradually becomes a steady state, showing a self-similar peeling. In recent research [13], the multiple peeling behavior of hyperelastic films has been widely discussed. The theoretical analysis adopts the constant displacement loading condition. Although the theoretical analysis method is different from above studies, the conclusion that the angle and force are constant after

* Corresponding author.
E-mail address: lengjs@hit.edu.cn (J. Leng).

https://doi.org/10.1016/j.eml.2023.102090
Received 17 August 2023; Received in revised form 28 September 2023; Accepted 7 October 2023
Available online 10 October 2023

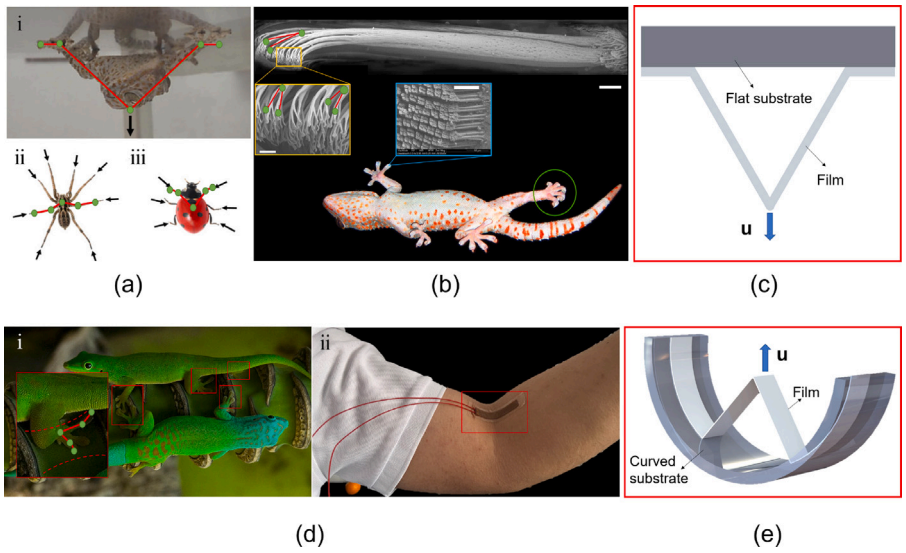

Fig. 1. (a) Macroscopic scale V-shape structures on flat substrates [13]: i Gecko, ii spider and iii lady bug; (b) Microscopic scale V-shape structures on flat substrates [20]; (c) Common characteristics regarding examples of V-shape structures peeling from flat substrate in (a) and (b); (d) Macroscopic scale V-shape structures on curved substrates: i Geckos on the curved surface of plant [21] and ii flexible electronics on curved arms; (e) Common characteristics regarding examples of V-shape structures peeling from curved substrate in (d).

stabilization is also obtained. It is not difficult to find that the VDP based on flat substrates has the similarity of steady-state peeling. After steady-state, peeling force and peeling angle does not change.

In fact, perfect flat substrates are rare, while substrates with uneven curved surfaces are more common, as shown in Fig. 1(d). However, only a few studies have been devoted to the peeling behavior of curved substrates [26–30]. For example, Peng et al. theoretically studied and analyzed the single peeling behavior of films on periodically sinusoidal surfaces and provided closed-form solutions for peeling force [28]. Deng et al. studied the single peeling of elastic films with large surface roughness on periodic surfaces and proposed a single peeling model for surfaces with arbitrary roughnesses [29]. Most existing curved substrate peeling studies have been focused on the analysis of single peeling behavior. The theoretical model of single peeling has a basic assumption that the direction of force is constant and the peeling arm is always highly parallel. Obviously, this assumption has limitations in studying the debonding behaviors of organisms.

As discussed above, VDP based on flat substrates will reach a steady state and peeling force and angle will not change, the peeling arm is always highly parallel for single peeling based on curved substrates. However, the VDP based on curved substrate is more complex, so the model of VDP from flat substrates and single peeling from curved substrates are no longer applicable. Meanwhile, VDP based on curved substrates can provide a more precise and profound model to explain the adhesion mechanism of geckos and other organisms in real life cases. Therefore, it is necessary to investigate the VDP behavior of films from curved substrates as shown in Fig. 1(e). The main content of this study are as follows: (1) A theoretical VDP model hyperelastic films from curved substrates is constructed; (2) The theoretical VDP results of hyperelastic films from curved rigid substrates are discussed and analyzed, and the influence of adhesion energy release rate and shear modulus of the film are considered; (3) The theoretical analysis of VDP from curved rigid substrates are verified through experimental tests and a new testing method of adhesion energy release rate is proposed.

2. Theoretical model of V-shaped double peeling from curved substrates

The scheme of VDP is depicted in Fig. 2. A homogeneous, incompressible, and isotropic hyperelastic film uniformly adheres to the inner surface a semi-cylindrical rigid curved substrate. Peeling occurs due to the vertical displacement. In this system, semi-cylindrical rigid substrate is fixed and constrained to be immovable with a center O and its radius is denoted as R. The film has a width of b and a thickness of t. Peeling between the film and the substrate initiates when a uniformly slow vertical displacement u is applied at the lowest point B of the adhesive interface. Simultaneously, the peeling point progresses forward along the arc of the substrate surface from point B for a distance L_1, which is peeling length. The process of peeling can be regarded as quasi-static. The film that has been dispatched from the substrate is called the peeling arm, which expands from the original length L_1 to the new length L_2. The peeling angle, denoted as α, is angle between L_2 and the tangent line of the substrate. β is angle between L_2 and u. The radian of the peeling length is denoted as θ. It is worth noting that the analysis only focuses on one half of the system due to the complete symmetry of the model and the thickness direction is not considered.

The Griffith's energy balance theory can be employed to describe the peeling of the film from the substrate and the following energy balance equation can be obtained

$$U_t = U_e + U_s, \tag{1}$$

where U_t is the external loading work, U_e is the elastic strain energy of the film, and U_s is the energy required to generate a new surface. In this problem, energy change due to film bending and energy loss due to friction and inertia can be neglected. Therefore, the energy change caused by debonding expansion can be written as

$$\frac{\partial(U_t - U_e)}{\partial A} = \frac{\partial U_s}{\partial A}, \tag{2}$$

where A is the debonded crack extension area and the right end of Eq. (2) is the energy release rate of debonded crack tip, which is the energy released per unit area of crack extension. Therefore, Eq. (2) defines energy release rate as

$$G = \frac{\partial(U_t - U_e)}{\partial A}. \tag{3}$$

G does not refer to a derivative with respect to time; G is the rate of change in potential energy with the crack area. Since G is obtained from the derivative of a potential, it is also called the crack extension force or the crack driving force. According to [31], G is usually calculated by displacement controlled or load controlled. In our study, displacement controlled was used, which is the same with the methods of Fraldi [13]

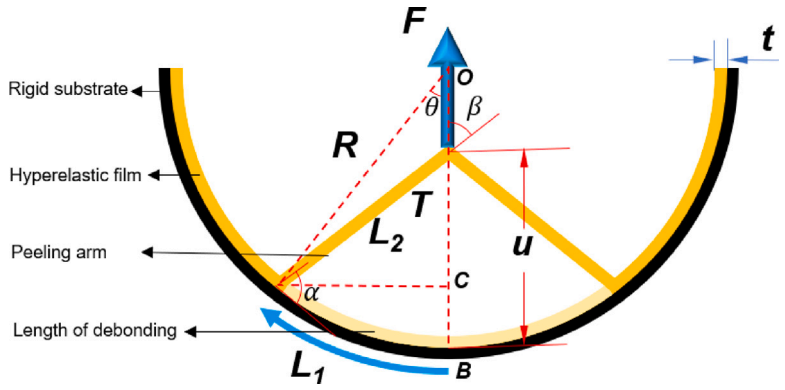

Fig. 2. The geometric parameters regarding V-shaped double peeling from a curved substrate.

and Hu [26]. When displacement controlled was used, Eq. (3) can be written as

$$G = -\frac{\partial U_e}{\partial A} = -\frac{\partial U_e}{\partial L_1} * \frac{1}{b}. \tag{4}$$

Assuming that the film is an isotropic, homogeneous, incompressible hyperelastic material, the constitutive equation can be expressed as

$$W = W(\lambda_1, \lambda_2, \lambda_3), \tag{5}$$

where W is the strain energy density. It is a function of principal stretch λ_1, λ_2 and λ_3. The principal first Piola–Kirchhoff stress can be easily derived [13]:

$$P_1 = \frac{\partial W}{\partial \lambda_1}, P_2 = \frac{\partial W}{\partial \lambda_2}, P_3 = \frac{\partial W}{\partial \lambda_3}. \tag{6}$$

We assumed that the debonded portion of the film is in uniaxial tensile stress state. Under this assumption, $P_1 = P$, $P_2 = P_3 = 0$, and λ_2 and λ_3 are both single-valued functions of λ. At the same time, $W = W(\lambda_1, \lambda_2, \lambda_3)$ and the first Piola–Kirchhoff stress $P = P(\lambda_1, \lambda_2, \lambda_3)$ are also single-valued functions, that is $W = W(\lambda)$ and $P = P(\lambda)$. For hyperelastic film, the simplest neo-hookean model [32] is used in this study. The elastic energy density under uniaxial tension is as follow [33]

$$W = \frac{\mu}{2}(\lambda^2 + \frac{2}{\lambda} - 3), \tag{7}$$

where μ is the shear modulus, and first Piola–Kirchhoff stress is

$$P = \mu(\lambda - \frac{1}{\lambda^2}). \tag{8}$$

The elastic strain energy of the peeling arm is

$$U_e = \int_{\Omega} W(\lambda) d\Omega = W(\lambda) L_1 bt. \tag{9}$$

Substituting Eq. (7) into Eq. (9)

$$U_e = \frac{\mu b t L_1}{2}(\lambda^2 + \frac{2}{\lambda} - 3), \tag{10}$$

where $\lambda = \frac{L_2}{L_1}$ is the elongation ratio of the peeling arm. The geometric relationship is

$$L_2^2 = [u - R(1 - \cos\theta)]^2 + (R\sin\theta)^2, \tag{11}$$

where $\theta = \frac{L_1}{R}$. Substituting Eqs. (10) and (11) into Eq. (4)

$$\frac{2G}{\mu t} = 3 - \frac{-2R^2 + 2Ru - u^2 + 2R(R-u)\cos\frac{L_1}{R}}{L_1^2} - \frac{2(R-u)\sin\frac{L_1}{R}}{L_1} + \frac{2L_1^2(R-u)\sin\frac{L_1}{R}}{[(-R+u+R\cos\frac{L_1}{R})^2 + (R\sin\frac{L_1}{R})^2]^{\frac{3}{2}}} - \frac{4L_1}{\sqrt{(-R+u+R\cos\frac{L_1}{R})^2 + (R\sin\frac{L_1}{R})^2}}. \tag{12}$$

Eq. (12), an implicit expression between u and L_1, is influenced by μ, t, G and R. To simplify Eq. (12), we transform the variables and parameters of Eq. (12) to dimensionless variables and parameters:

$$\bar{G} = 3 - \frac{-2 + 2\bar{u} - \bar{u}^2 + 2(1-\bar{u})\cos\bar{L}_1}{\bar{L}_1^{\,2}} - \frac{2(1-\bar{u})\sin\bar{L}_1}{\bar{L}_1} + \frac{2\bar{L}_1^{\,2}(1-\bar{u})\sin\bar{L}_1}{[(-1+\bar{u}+\cos\bar{L}_1)^2 + (\sin\bar{L}_1)^2]^{\frac{3}{2}}} - \frac{4\bar{L}_1}{\sqrt{(-1+\bar{u}+\cos\bar{L}_1)^2 + (\sin\bar{L}_1)^2}}, \tag{13}$$

where $\bar{u} = \frac{u}{R}$, $\bar{G} = \frac{2G}{\mu t}$ and $\bar{L}_1 = \frac{L_1}{R}$.

When the peeing is extended to $\bar{u} = 1$, $(1-\bar{u})\sin\bar{L}_1 = 0$ and $(1-\bar{u})\cos\bar{L}_1 = 0$. Eq. (13) becomes

$$\bar{G} = 3 + \frac{1}{\bar{L}_1^{\,2}} - 4\bar{L}_1. \tag{14}$$

Eq. (14) is a simplification of Eq. (13). The adhesion energy release rate, G, is a function of $\bar{L}_1$. This approach presents a new and simplified method for measuring the energy release rate of adhesion, without the need for direct measurement of peeling force loading. It is detailed discussed in Section 4.

3. Results and discussion

3.1. The variation of peeling length with vertical displacement

Eq. (13) can be solved for the given $\bar{u}$ to obtain the corresponding $\bar{L}_1$. The curve of the $\bar{L}_1$ relative to the $\bar{u}$ can be plotted, as shown in Fig. 3. When the value of $\bar{G}$ is smaller, such as 1, the expansion of peeling gradually decelerates as the increase of $\bar{u}$. The relationship between $\bar{u}$ and $\bar{L}_1$ is nonlinear. Because the geometric nonlinearity of the peeling system plays a leading role in the peeling process. Examining an extreme case: when the value of $\bar{G}$ equals 0, represented by the red line in Fig. 3, the entire peeling process becomes purely geometric relationship. In this case, there is no stretch of the peel arm and the length of the peel arm L_2 is equal to L_1. When $L_1 = L_2$, according to Eq. (11),

$$(\frac{L_1}{R})^2 = [\frac{u}{R} - (1 - \cos\frac{L_1}{R})]^2 + (\sin\frac{L_1}{R})^2 = (\frac{u}{R} - 1)^2 + 2(\frac{u}{R} - 1)cos\frac{L_1}{R} + 1. \tag{15}$$

Therefore,

$$(\bar{u} - 1)^2 + 2(\bar{u} - 1)\cos\bar{L}_1 + 1 = \bar{L}_1^{\,2}. \tag{16}$$

The nonlinearity in the relationship between $\bar{u}$ and $\bar{L}_1$ is solely due to geometric factors. It should be noted that this theoretical model does not consider the bending of the peeling arm. However, when the value of $\bar{G}$ is larger, such as 5 and 10, the relationship between $\bar{u}$ and $\bar{L}_1$ tends to be linear. In this case, peeling is difficult to expand forward. Even if

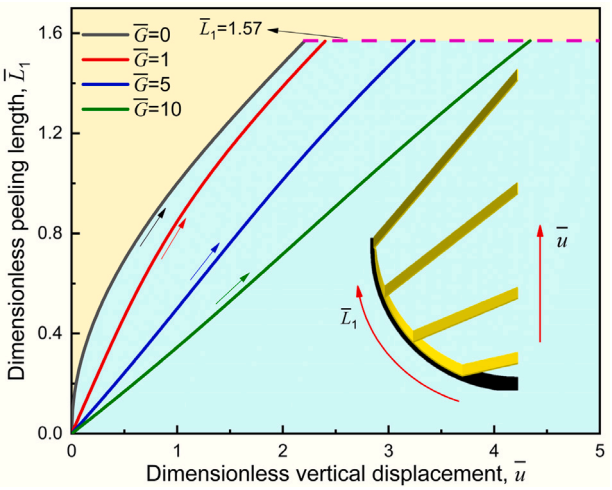

Fig. 3. The dimensionless peeling length $\bar{L}_1$ vs. dimensionless vertical displacement $\bar{u}$. (For interpretation of the references to color in this figure legend, the reader is referred to the web version of this article.)

$\bar{u}$ is larger, $\bar{L}_1$ is still smaller. Therefore, $\bar{u}$ is an infinitesimal quantity relative to $\bar{L}_1$ and in this case,

$$\frac{2\bar{L}_1{}^2(1-\bar{u})\sin\bar{L}_1}{[(-1+\bar{u}+\cos\bar{L}_1)^2+(\sin\bar{L}_1)^2]^{\frac{3}{2}}} \ll (\frac{\bar{u}}{\bar{L}_1})^2. \tag{17}$$

$$\frac{4\bar{L}_1}{\sqrt{(-1+\bar{u}+\cos\bar{L}_1)^2+(\sin\bar{L}_1)^2}} \ll (\frac{\bar{u}}{\bar{L}_1})^2. \tag{18}$$

$$\frac{2(1-\bar{u})\sin\bar{L}_1}{\bar{L}_1} \ll (\frac{\bar{u}}{\bar{L}_1})^2. \tag{19}$$

$$\frac{-2+2\bar{u}+2(1-\bar{u})\cos\bar{L}_1}{\bar{L}_1{}^2} \ll (\frac{\bar{u}}{\bar{L}_1})^2. \tag{20}$$

Therefore, a simplification of Eq. (13) is

$$\sqrt{\bar{G}-3}=\frac{\bar{u}}{\bar{L}_1}, \tag{21}$$

According Eq. (21), it can be found that the relationship between $\bar{u}$ and $\bar{L}_1$ tends to be linear. On the other hand, as the value of $\bar{G}$ tends to ∞, the line where $\bar{L}_1$ varies with $\bar{u}$ will be infinitely close to the horizontal axis.

3.2. The variation of angle with vertical displacement

The peeling angle α can be calculated by

$$\alpha=\frac{\pi}{2}+\bar{L}_1-arctan(\frac{sin\bar{L}_1}{\bar{u}-1+cos\bar{L}_1}). \tag{22}$$

Fig. 4 illustrates the relationship between peeling angle and dimensionless vertical displacement, with different lines representing various values of $\bar{G}$. When $\bar{G}=0$, the value of α gradually increases non-linearly as $\bar{u}$ increases, and the increasing speed becomes slow. In this case, the adhesion surface energy is zero, and the film and the substrate do not slide. The pure geometric relationship leads to the nonlinear relationship between α and $\bar{u}$, which is similar to Section 3.1. When $\bar{G}>0$, the value of α quickly reaches a large value with a small increase in $\bar{u}$ and then increases nonlinearly with the continued increase in $\bar{u}$. It is because in the initial stage, as long as there is a small peeling expansion, the peeling arm will have a great stretch and lead to a large peeling angle. However, when values of $\bar{G}$ is larger (for example, $\bar{G}>5$), the relationship between α and $\bar{u}$ is almost linear. In this case, $\bar{u}$ is an infinitesimal quantity relative to $\bar{L}_1$. Therefore, in Eq. (22), α can be simplified as a linear function of $\bar{L}_1$. Therefore, when the value of $\bar{G}$ is larger the relationship between $\bar{u}$ and $\bar{L}_1$ tends to be linear and there is an almost linear relationship between α and $\bar{u}$. Regardless of the value of $\bar{G}$, the curve passes through a point where $\bar{u}=1$ and $\alpha=\frac{\pi}{2}$. This point is significant as it corresponds to Eq. (13) simplified to Eq. (14). Beyond this point, the peeling angle will be greater than $\frac{\pi}{2}$, which is not possible for VDP from flat substrates. For VDP from curved substrates, with the progress of peeling, peeling angle will always change. VDP from curved substrates does not become similar peeling state, which is different from flat substrates.

The relationship between the angle β and the vertical displacement $\bar{u}$ is given by Eq. (23)

$$\beta=arctan(\frac{sin\bar{L}_1}{\bar{u}-1+cos\bar{L}_1}). \tag{23}$$

By plotting the dimensionless displacement $\bar{u}$ as the abscissa and β as the ordinate, the curve shown in Fig. 4 is generated, with different lines representing various values of $\bar{G}$. When $\bar{G}=0$, the film does not adhere to the substrate. The relationship is purely geometric. As $\bar{u}$ increases, β nonlinearly increases, and the increase speed becomes slow. For the case, where $\bar{G}>0$, as $\bar{u}$ increases, β initially increases and then decreases in a nonlinear fashion, with the existence of a maximum value during this process. β depends on the swing of peeling arm.

3.3. The variation of stretch and peeling force with vertical displacement

By substituting $\lambda=\frac{L_2}{L_1}$ and $\theta=\frac{L_1}{R}$ into Eq. (11), the dimensionless implicit expression of stretch λ as a function of $\bar{u}$ can be obtained

$$(\lambda\bar{L}_1)^2=[\bar{u}-(1-\cos\bar{L}_1)]^2+(R\sin\bar{L}_1)^2. \tag{24}$$

In Section 3.1, $\bar{L}_1$ is a function of $\bar{u}$, which has been calculated. Take $\bar{u}$ as the abscissa and the corresponding the λ as the ordinate to draw the curve, as shown in Fig. 5(a). It can be observed that the stretch of the peeling arm λ initially increases rapidly to a maximum value at the beginning of peeling and then decreases gradually. In addition, the rate of decrease becomes slower as the peeling process proceeds. It is because that the peeling angle increases and peeling becomes easier.

The dimensionless tension force $\bar{T}$ of the peeling arm is a function of λ

$$\bar{T}=\lambda-\frac{1}{\lambda^2}, \tag{25}$$

where $\bar{T}=\frac{T}{\mu bt}$ and T is the tension force of the peeling arm. Fig. 5(b) shows the dimensionless tension force curve, where the dimensionless displacement $\bar{u}$ is the abscissa, and the dimensionless tension force $\bar{T}$ is the ordinate. It can be observed that $\bar{T}$ initially increases rapidly, reaching a maximum value. As the peeling progresses, the tension force gradually decreases. Moreover, the rate of decrease slows down, which is consistent with the trend observed in the stretch of the peeling arm.

The expression of dimensionless vertical peeling force is

$$\bar{F}=\cos\beta(\lambda-\frac{1}{\lambda^2}), \tag{26}$$

where $\bar{F}=\frac{F}{\mu bt}$ and F is vertical peeling force.

Fig. 4(c) illustrates the relationship between the $\bar{F}$ and $\bar{u}$. The trend of the dimensionless vertical peeling force is similar to that of the dimensionless tension force. VDP based on curved substrates is different from that of flat substrates. In the case of VDP from the flat substrate, as described in the work of Fraldi et al. [13], the vertical peeling force initially increases rapidly and then reaches a stable value that remains constant as u increases. However, in the case of VDP from the curved substrate, the vertical peeling force gradually decreases, which is attributed to the change of α. The studies of VDP based on the flat substrate [12,13] have shown that the peeling does not occur when peeling angle is below maximum threshold. An increase in peeling force results in an increase in peeling angle, resulting in peeling. The peeling force is closely related to the peeling angle. For instance, geckos require the peeling angle of less than 30° to prevent falling, whereas adjusting it beyond 30° promotes rapid debonding [3].

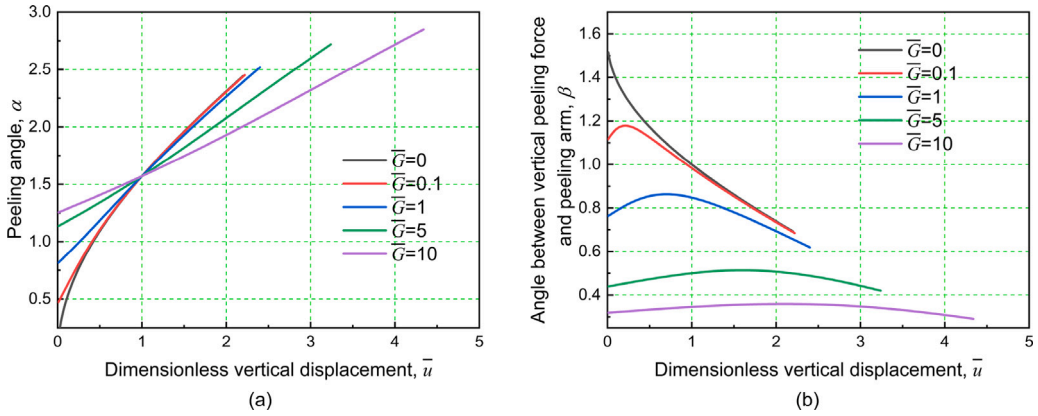

Fig. 4. The variation of angle with dimensionless vertical displacement: (a) peeling angle α, (b) angle between vertical tensile force and peeling arm β.

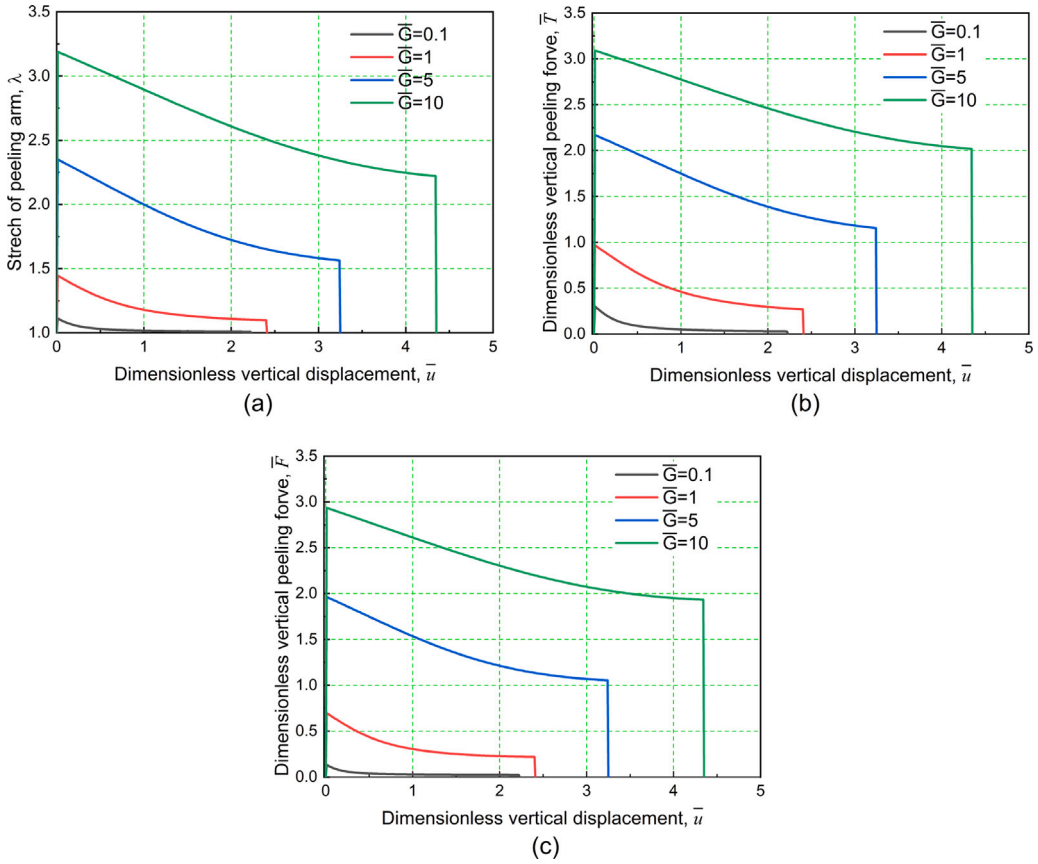

Fig. 5. The dimensionless stretch and force vs. dimensionless vertical displacement: (a) dimensionless stretch, (b) dimensionless tension force, (c) dimensionless vertical peeling force.

3.4. The variation of energy with vertical displacement

The relationship between dimensionless energy $\bar{U} = \frac{U}{\mu b t R}$ and dimensionless vertical displacement $\bar{u}$ is shown in Fig. 6. It should be noted that we theoretically assume that the crack tends to be infinitely small, so surface energy is depicted throughout the whole peeling process. The different curves represent the external work, strain energy and surface energy during the peeling process of different $\bar{G}$. The external work is the sum of the strain energy and surface energy. Regardless of the value of $\bar{G}$, both the external work and surface energy gradually increase as the peeling progresses and the rate of increase slows down. When $\bar{G}$ is smaller, nonlinear relationship between energy and displacement becomes more apparent. Strain energy differs from the external work and surface energy and its trend is strongly influenced by the value of $\bar{G}$. When $\bar{G} = 0.1$ and 1, the strain energy initially increases with the increase of $\bar{u}$, and the rate of increase gradually slows down. Subsequently, the strain energy reaches a maximum value, and then the strain energy starts to decrease. For relatively large values of $\bar{G}$, such as 5 and 10, the strain energy increases with the increase of $\bar{u}$, but the rate of increase slows down. This indicates a strong adhesive situation, and the curve resembles the scenario of single tensile loading of a hyperelastic film.

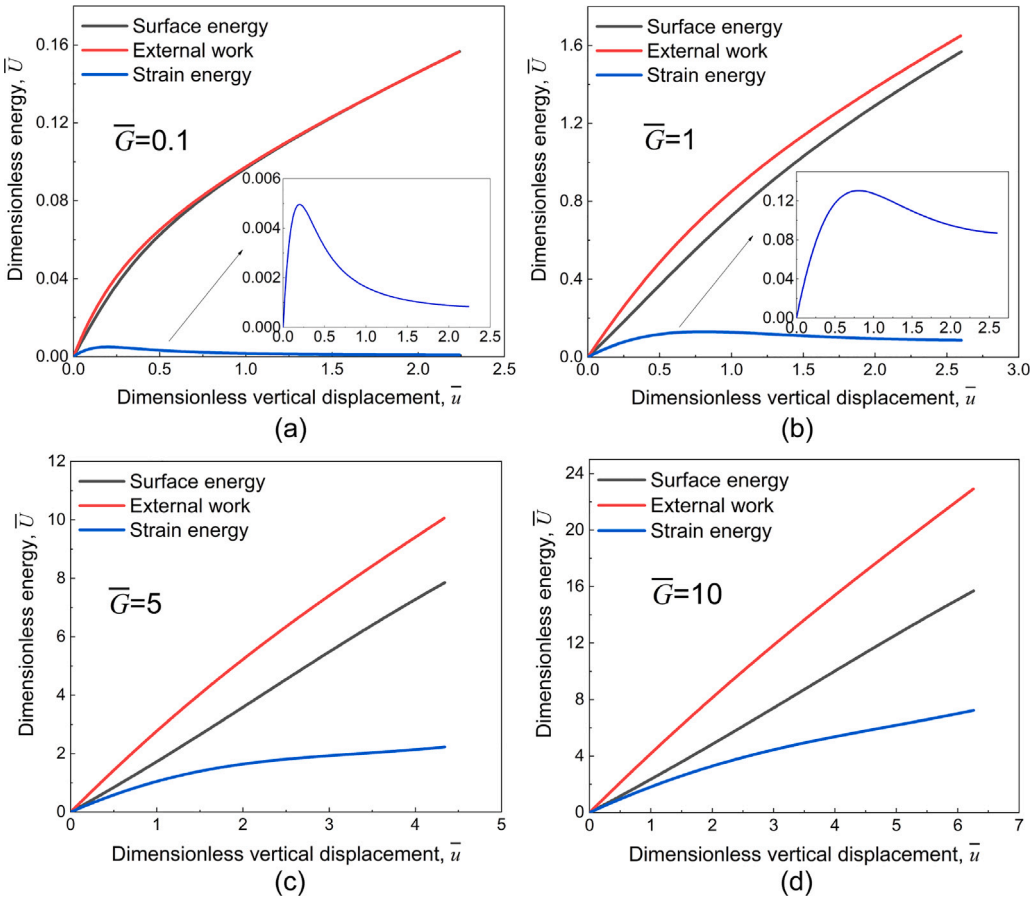

Fig. 6. The dimensionless energy vs. dimensionless vertical displacement: (a) $\bar{G} = 0.1$, (b) $\bar{G} = 1$, (c) $\bar{G} = 5$, (d) $\bar{G} = 10$.

4. Experimental verification of VDP and a new test method of adhesion energy release rate

4.1. Experimental verification of VDP

The information of the materials and devices used in the VDP tests is given in Appendix. For the VDP test, the inner surface of the substrate and the film were uniformly coated with adhesive, and then pressure was applied using a pressure wheel (2 kg) to ensure uniform bonding. Finally, samples were prepared by standing and curing at room temperature for 3 h. The sample is mounted on a special fixture as shown in Fig. 7 for peeling test. The SHIMADZU AGS-X mechanical testing machine was used for VDP test and the moving speed is 25 mm/min. In this paper, we think that the peeling process is a quasi-static process, and the whole peeling process is considered to be composed of multiple crack propagation modes with displacement controlled, and each crack propagation is a static displacement controlled mode. During the VPD test, the peeling length was determined by capturing the scale on one side of the curved substrate. As shown in Fig. 7, the sample remained intact at 0 s, and then a displacement was applied to initiate the peeling. At a displacement of $u = R$ (240 s), the corresponding angle was measured as 35°. The peeling continued until 645 s, at which point the film fully detached.

Simultaneously, experimental results of vertical peeling force and vertical displacement were recorded in Fig. 8 and the blue line represents the average values of three samples. The adhesion energy release rate can be calculated using the same method of Li [34]. Based on the test results, the adhesion energy release rates for the three samples are $G_{01} = 0.35$ N/mm, $G_{02} = 0.36$ N/mm and $G_{03} = 0.32$ N/mm, and the average value of the energy release rate of adhesion is $G_0 = 0.34$ N/mm. The red line, in Fig. 8, represents the theoretical values with $\mu = 0.25$ MPa, $t = 1$, and $G = 0.34$ N/mm. There is a good agreement between experimental and theoretical results, which proves the validity of the theoretical model.

4.2. Test method of adhesion energy release rate based on curved substrates

For the case of flat peeling, when bending stiffness of the film is negligible and tensile stiffness is infinite, the adhesion energy release rate can be easily measured of using a material stretch tester with a substrate moving device. However, when tensile stiffness of the film is not infinite, the problem becomes more complicated. As mentioned in [35], the peeling angle constantly changes, leading to measurement errors. To solve this problem, a common approach is to attach a backplane with smaller bending stiffness and infinite tensile stiffness to the backside of the stretchable film. In addition, this test method still requires the coordination of a complex substrate moving device. A new method for measuring the adhesion energy release rate of stretchable films is proposed.

This method is as follow. First, uniformly adhere a film with a known thickness and shear modulus to a rigid substrate with a radius of R. Then pull the film along the radius slowly and uniformly. During this process, the peeling length L_1 is recorded when the vertical displacement u equals the radius R. Finally, Use the peel measurement data L_1 to calculate adhesion energy release rate according to the explicit expression

$$G = \frac{\mu t}{2}\left(3 + \frac{R^2}{L_1^2} - \frac{4L_1}{R}\right). \tag{27}$$

Eq. (27) is equivalent to Eq. (14).

This method is simple, convenient and easy to perform without the need for a peeling force testing machine and a substrate moving device.

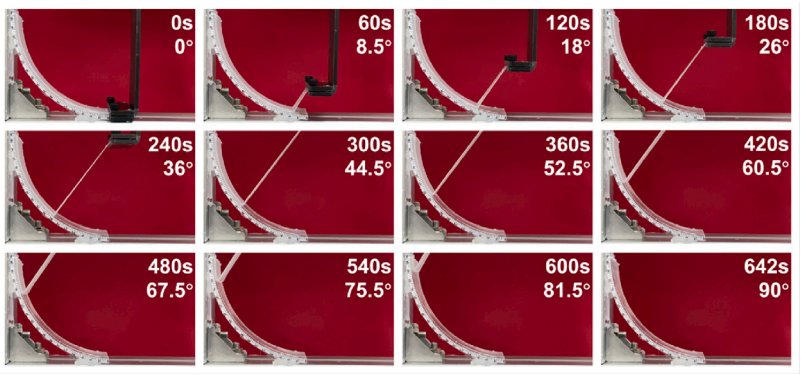

Fig. 7. VDP test of a film from a curved rigid substrate.

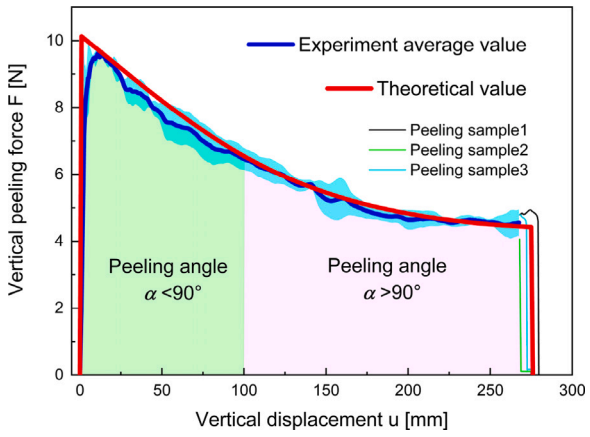

Fig. 8. Vertical peeling force vs. vertical displacement. (For interpretation of the references to color in this figure legend, the reader is referred to the web version of this article.)

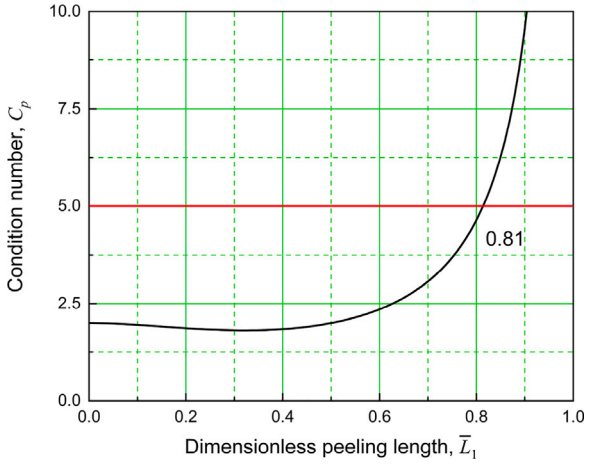

Fig. 9. Condition number vs. dimensionless peeling length.

Noting that there are two cases that our method may not be suitable for hyperelastic materials with strong adhesion involving large process zones and strong adhesion that no delamination occurs. Because, for peeling with large process zone involving complicated crack-tip deformation field [36,37], the geometric relationship in Eq. (11) may not accurate enough. When the adhesion between the film and substrate is strong enough that no delamination occurs, Eq. (14) may overestimate the value of G. The newly proposed energy release rate test method is applied to process the test results obtained in the previous Section 4.1. The adhesive energy release rates for the three tests are $G_{11} = 0.36$ N/mm, $G_{12} = 0.38$ N/mm and $G_{13} = 0.35$ N/mm, with an average value is $G_1 = 0.36$ N/mm. The relative error obtained from the new method is 5.88%.

4.3. Sensitivity analysis of the new test method

Sensitivity analysis is a method of system stability evaluation. According to Eq. (27), the adhesion energy release rate G is a function of four variables

$$G = f(\mu, t, L_1, R), \tag{28}$$

where μ, t and R are the known variables, and L_1 is the measured variable. A dimensionless sensitivity analysis should be used to analyze sensitivity. Use the Π theorem for Eq. (28)

$$\frac{G}{\mu t} = \Pi\left(\frac{L_1}{R}\right), \tag{29}$$

where Π is dimensionless function. According to Eq. (27)

$$\Pi = 3 + \frac{1}{\bar{L}_1^{\,2}} - 4\bar{L}_1. \tag{30}$$

The condition number of a problem can measure sensitivity of identified parameter to small changes in input data. The condition number can be calculated by

$$C_p = \frac{\Delta \bar{L}_1}{\bar{L}_1} \Big/ \frac{\Delta \Pi}{\Pi} = \frac{4\bar{L}_1^{\,3} + 2}{4\bar{L}_1^{\,3} - 3\bar{L}_1^{\,2} - 1}, \tag{31}$$

where C_p is condition number. C_p varying with $\bar{L}_1$ is shown as Fig. 9.

When $\bar{L}_1$ is smaller than 0.5, the value of C_p is 2, which is basically unchanged. Then, with the increase of $\bar{L}_1$, the value of C_p becomes gradually larger, and until $\bar{L}_1$ is less than 0.81, the value of C_p is always lower than 5. In this case, a smaller error of $\bar{L}_1$ will not lead to larger error of G and it is a well-conditioned problem.

5. Conclusions

V-shaped double peeling (VDP) behavior of films from curved substrates is investigated via theoretical analysis, which is confirmed through experimental validation. Firstly, a VDP theoretical model for hyperelastic thin films on semi-cylindrical curved rigid substrates based on the energy based Griffith fracture criterion is derived. An implicit expression is provided to determine the peeling length and vertical displacement. Subsequently, by solving for the peeling length under given vertical displacement conditions, the relationship between delamination length and vertical displacement is studied. When the value of $\bar{G}$ is smaller, there is a nonlinear correlation between the

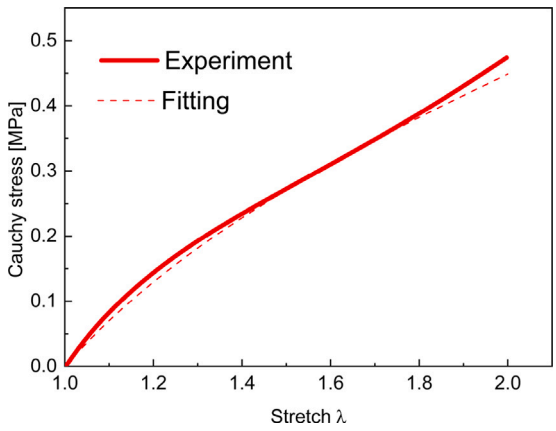

Fig. 10. Stress–stretch curve of the hyperelastic film under uniaxial stress regime.

peeling length and vertical displacement. However, it approaches a linear relationship when $\bar{G}$ is larger. Furthermore, the peeling angle and vertical peeling force are studied. The peeling angle increases continuously with an increase in vertical displacement. In contrast to flat VDP, where peeling angle remains constant, peeling behavior of VDP based on curved substrates is more complex and dissimilar. As peeling angle increases, peeling force decreases as expected, making peeling process more likely to occur. This is different from the constant peeling force in flat VDP. In order to validate the theoretical model, experimental tests are carried out, and the result prove the effectiveness of the theoretical model. Finally, based on the VDP theory of curved substrates, a test method is proposed to evaluate the adhesive properties of films on rigid substrates, and the sensitivity analysis of the test method is carried out. This method is simple and easy to implement without using a force test unit.

This work contributes to understanding adhesion mechanisms of organisms like geckos on curved surfaces, which holds the potential for the design of novel biomimetic adhesive systems. Furthermore, this work offers new insights to testing the adhesive properties of soft materials. However, further research is needed for materials exhibiting viscoelastic behaviors.

Declaration of competing interest

The authors declare that they have no known competing financial interests or personal relationships that could have appeared to influence the work reported in this paper.

Data availability

Data will be made available on request.

Appendix. Materials and devices used in the VDP tests

In this study, the rigid substrate was made of glass with an inner diameter of 200 mm, which was provided by Donghai Haotian Quartz Glass Products Co., Ltd. Angular scales were set on the side of the substrate to facilitate the measurement of peeling length L_1. The adhesive was Kraft K-705 silicone. 1 mm thick and 3 mm wide hyperelastic silicone rubber produced by Guangdong Zhongying Plastic Products Co., Ltd. was used for experiment. The shear modulus of the film was determined using the SHIMADZU AGS-X mechanical testing machine with a maximum range of 100 N. The test speed was set at 25 mm/min. Fig. 10 shows an example of such a test. The shear modulus was obtained by fitting, and the results of the three tests were 0.24 MPa, 0.26 MPa and 0.25 MPa, respectively, with an average value of 0.25 MPa.

References

[1] S. Baik, H.J. Lee, D.W. Kim, J.W. Kim, Y. Lee, C. Pang, Bioinspired adhesive architectures: From skin patch to integrated bioelectronics, Adv. Mater. 31 (34) (2019) 1803309.
[2] Z. Zhu, Z. Yang, Y. Xia, H. Jiang, A review of debonding behavior of soft material adhesive systems, Mech. Mater. 4 (1) (2022) 7.
[3] W. Duan, Z. Yu, W. Cui, Z. Zhang, W. Zhang, Y. Tian, Bio-inspired switchable soft adhesion for the boost of adhesive surfaces and robotics applications: A brief review, Adv. Colloid Interface Sci. (2023) 102862.
[4] Z. Li, X. He, J. Cheng, H. Li, Y.-F. Zhang, X. Shi, K. Yu, H.Y. Yang, Q. Ge, Hydrogel-elastomer-based stretchable strain sensor fabricated by a simple projection lithography method, Int. J. Smart Nano Mater. 12 (3) (2021) 256–268.
[5] V. Chiaula, J. Jeppe Madsen, F. Madsen, P. Mazurek, A. Nielsen, A. Skov, Antimicrobial silicone skin adhesives facilitated by controlled octenidine release from glycerol compartments, Int. J. Smart Nano Mater. (2023) 1–21.
[6] K. Autumn, Y.A. Liang, S.T. Hsieh, W. Zesch, W.P. Chan, T.W. Kenny, R. Fearing, R.J. Full, Adhesive force of a single gecko foot-hair, Nature 405 (6787) (2000) 681–685.
[7] A.J. Ijspeert, Biorobotics: Using robots to emulate and investigate agile locomotion, Science 346 (6206) (2014) 196–203.
[8] E. Pennisi, Geckos climb by the hairs of their toes, Science 288 (5472) (2000) 1717–1718.
[9] J. Liu, Y. Yao, S. Chen, X. Li, Z. Zhang, A strong and reversible adhesive fibrillar surface based on an advanced composite with high strength and strong adhesion, Int. J. Smart Nano Mater. 14 (1) (2023) 103–121.
[10] D. Misseroni, L. Afferrante, G. Carbone, N. Pugno, Non-linear double-peeling: Experimental vs. theoretical predictions, J. Adhes. 94 (1) (2018) 46–57.
[11] L. Afferrante, G. Carbone, G. Demelio, N. Pugno, Adhesion of elastic thin films: Double peeling of tapes versus axisymmetric peeling of membranes, Tribol. Lett. 52 (2013) 439–447.
[12] N.M. Pugno, The theory of multiple peeling, Int. J. Fract. 171 (2011) 185–193.
[13] M. Fraldi, S. Palumbo, A. Carotenuto, A. Cutolo, N. Pugno, Generalized multiple peeling theory uploading hyperelasticity and pre-stress, Extreme Mech. Lett. 42 (2021) 101085.
[14] C. Putignano, L. Afferrante, L. Mangialardi, G. Carbone, Equilibrium states and stability of pre-tensioned adhesive tapes, Beilstein J. Nanotechnol. 5 (1) (2014) 1725–1731.
[15] L. Heepe, S. Raguseo, S.N. Gorb, An experimental study of double-peeling mechanism inspired by biological adhesive systems, App. Phys. A 123 (2017) 1–8.
[16] L. Brely, F. Bosia, N.M. Pugno, Numerical implementation of multiple peeling theory and its application to spider web anchorages, Interface Focus 5 (1) (2015) 20140051.
[17] N. Menga, L. Afferrante, N. Pugno, G. Carbone, The multiple V-shaped double peeling of elastic thin films from elastic soft substrates, J. Mech. Phys. Solids 113 (2018) 56–64.
[18] L. Brely, F. Bosia, S. Palumbo, M. Fraldi, A. Dhinojwala, N.M. Pugno, Competition between delamination and tearing in multiple peeling problems, J. R. Soc. Interface 16 (160) (2019) 20190388.
[19] L. Heepe, L. Xue, S.N. Gorb, Biological Prototypes, Fabrication, Tribological Properties, Contact Mechanics, and Novel Concepts, in: Bio-Inspired Structured Adhesives, Vol. 9, Springer, 2017.
[20] K. Autumn, A. Dittmore, D. Santos, M. Spenko, M. Cutkosky, Frictional adhesion: A new angle on gecko attachment, J. Exp. Biol. 209 (18) (2006) 3569–3579.
[21] A.V. Mohan, P. Orozco-terWengel, K. Shanker, M. Vences, The Andaman day gecko paradox: An ancient endemic without pronounced phylogeographic structure, Sci. Rep. 10 (1) (2020) 11745.
[22] H. Gao, X. Wang, H. Yao, S. Gorb, E. Arzt, Mechanics of hierarchical adhesion structures of geckos, Mech. Mater. 37 (2–3) (2005) 275–285.
[23] B. Bhushan, Gecko feet: natural hairy attachment systems for smart adhesion–mechanism, modeling and development of bio-inspired materials, Nanotribology and Nanomechanics, Springer, 2008, pp. 1073–1134.
[24] K. Kendall, Thin-film peeling-the elastic term, J. Phys. D: Appl. Phys. 8 (13) (1975) 1449–1452.
[25] P. Gialamas, B. Völker, R.R. Collino, M.R. Begley, R.M. McMeeking, Peeling of an elastic membrane tape adhered to a substrate by a uniform cohesive traction, Int. J. Solids Struct. 51 (18) (2014) 3003–3011.
[26] Y. Hu, J. Leng, F. Jia, Y. Liu, Peeling behavior of a film on inner surface of a tube, Extreme Mech. Lett. 58 (2023) 101930.
[27] O. Kruglova, F. Brau, D. Villers, P. Damman, How geometry controls the tearing of adhesive thin films on curved surfaces, Phys. Rev. Lett. 107 (16) (2011) 164303.
[28] Z. Peng, S. Chen, Peeling behavior of a thin-film on a corrugated surface, Int. J. Solids Struct. 60 (2015) 60–65.
[29] W. Deng, H. Kesari, Angle-independent optimal adhesion in plane peeling of thin elastic films at large surface roughnesses, J. Mech. Phys. Solids 148 (2021) 104270.

[30] X. Ma, H. Long, Y. Wei, Self-debonding of adhesive thin films on convex cylindrical surfaces and spherical surfaces, Int. J. Appl. Mech. (2023) 1–23.
[31] T.L. Anderson, Fracture Mechanics: Fundamentals and Applications, CRC Press, 2017.
[32] E.M. Arruda, M.C. Boyce, A three-dimensional constitutive model for the large stretch behavior of rubber elastic materials, J. Mech. Phys. Solids 41 (2) (1993) 389–412.
[33] C. Chen, Z. Wang, Z. Suo, Flaw sensitivity of highly stretchable materials, Extreme Mech. Lett. 10 (2017) 50–57.
[34] Q. Li, W. Liu, C. Yang, P. Rao, P. Lv, H. Duan, W. Hong, Kirigami-inspired adhesion with high directional asymmetry, J. Mech. Phys. Solids 169 (2022) 105053.
[35] X. Li, R. Tao, Y. Xin, G. Lubineau, Cassette-like peeling system for testing the adhesion of soft-to-rigid assemblies, Int. J. Solids Struct. 251 (2022) 111751.
[36] Y. Jia, Z. Zhou, H. Jiang, Z. Liu, Characterization of fracture toughness and damage zone of double network hydrogels, J. Mech. Phys. Solids 169 (2022) 105090.
[37] Z. Zhou, J. Lei, Z. Liu, Effect of water content on physical adhesion of polyacrylamide hydrogels, Polymer 246 (2022) 124730.